Transmission Tomography Reconstruction Using Compound Gauss-Markov Random Fields and Ordered Subsets *

A. López[1], J. M. Martín[2], R. Molina[2], and A. K. Katsaggelos[3].

[1] Departamento de Lenguajes y Sistemas Informáticos, Universidad de Granada, 18071 Granada, Spain alopez@ugr.es
[2] Departamento de Ciencias de la Computación e I.A., Universidad de Granada, 18071 Granada, Spain jmartin,rmsn@decsai.ugr.es
[3] Northwestern University, Department of Electrical Engineering and Computer Science
Evanston, Illinois 60208-3118 aggk@ece.northwestern.edu

Abstract. Emission tomography images are degraded due to the presence of noise and several physical factors, like attenuation and scattering. To remove the attenuation effect from the emission tomography reconstruction, attenuation correction factors (ACFs) are used. These ACFs are obtained from a transmission scan and it is well known that they are homogeneous within each tissue and present abrupt variations in the transition between tissues. In this paper we propose the use of compound Gauss Markov random fields (CGMRF) as prior distributions to model homogeneity within tissues and high variations between regions. In order to find the maximum *a posteriori* (MAP) estimate of the reconstructed image we propose a new iterative method, which is stochastic for the line process and deterministic for the reconstruction. We apply the ordered subsets (OS) principle to accelerate the image reconstruction. The proposed method is tested and compared with other reconstruction methods.

1 Introduction

The attenuation or absorption of photons is an important effect in PET (positron emission tomography) and SPECT (single photon emission tomography) systems, that produces errors by decreasing the quantitative accuracy of the reconstructed emission image [7]. Reliable attenuation correction methods for emission tomography require determination of an attenuation map, which represents the spatial distribution of ACFs. Frequently, the attenuation correction is performed from a transmission scan that determines the tissue structure in a patient. The transmission scan can be either previous (pre-injection measurements) or simultaneous to the emission scan (post-injection measurements).

* This work has been partially supported by "Instituto de Salud Carlos III" projects FIS G03/185, and FIS PI040857 and by the "Comisión Nacional de Ciencia y Tecnología under contract TIC2003-00880.

Bayesian reconstruction methods have been extensively used to reconstruct medical images since they can improve the reconstructions with respect to the classical, non statistical methods, such as FBP (filtered back projection) [11] and ART (algebraic reconstruction techniques) [17].

In the Bayesian paradigm, the reconstructed image $\hat{X}$ is obtained according to

$$\hat{X} = \arg\max_X P(X|Y) = \arg\max_X P(Y|X)P(X), \tag{1}$$

where $P(X)$ is a prior distribution incorporating the expected structure in the image X, and $P(Y|X)$ is a likelihood for projection data Y which depends on the real underlying image X, and models the formation process of projections. For transmission reconstruction, nonquadratic prior distributions are extensively used [4, 21], since these priors allow to model the existence of anatomical edges.

In this work, we propose a Bayesian reconstruction method that uses compound Gauss-Markov prior models to reconstruct attenuation maps for pre-injection measurements. Furthermore, we have adopted the ordered subsets (OS) [9] technique for projection data to accelerate the proposed transmission reconstruction algorithm. Applying OS, an iterative method processes the projection data in subsets within each iteration instead of using the whole data set. The OS algorithms are perhaps the most frequently used to improve the convergence rate of statistical reconstruction methods.

The rest of the paper is organized as follow. In section 2 we define the degradation and image models. Then, in section 3 we propose a method for finding the MAP estimate. The application of this method to real images is described in section 4. Finally, section 5 concludes the paper.

2 Degradation and Image Models

In order to define the degradation distribution $P(Y|X)$, we note that in transmission tomography the attenuation is independent of position along the projection line and the observation data and is specified by Poisson distributions (pre-injection measurements), i.e.,

$$P(Y|X) \propto \prod_{i=1}^{M} \left[\exp\{-b_i e^{-c_i}\}\right] \left(b_i \exp\{c_i\}\right)^{y_i}, \tag{2}$$

where

$$c_i = \sum_{j=1}^{N} A_{i,j} x_j,$$

and M is the number of detectors, N the number of pixels, and A the $M \times N$ system matrix. $A_{i,j}$ is the intersection length of the projection line i with the

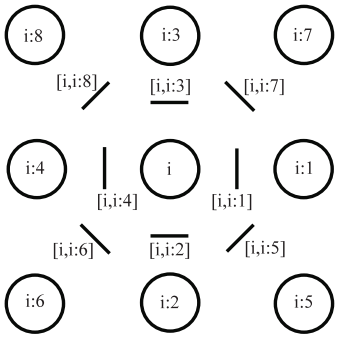

Fig. 1. Image and line sites

area represented by pixel j, x_j represents the attenuation correction factor at pixel j, b_i is the blank scan count, y_i is the number of transmission counts at the ith detector pair in PET or detector in SPECT and c_i represents a line integral of the attenuation map X. We note that in this distribution the random coincidences are ignored.

We use a CGMRF distribution as image model. This prior has been previously applied, for instance, to multichannel image restoration [16] and emission SPECT reconstruction problems [13]. A CGMRF model provides us with a means to control changes in the image using an auxiliary random field. This model has two levels, an upper level which is the image to be restored and a lower or auxiliary level that it is a finite range random field to govern the transition between the sub-models. The use of an underlying random field, called the line process, was introduced by Geman and Geman [6] in the discrete case. Extensions to the continuous case were presented by Jeng and Woods [10].

The CGMRF model is introduced from a simpler one, the conditional autoregression (CAR) model [18], which is defined by

$$P(X) \propto \exp\{-\frac{1}{2}\alpha\, X^t(I-\phi C)X\}, \tag{3}$$

where α is a scaling parameter which adjusts the global smoothness of the reconstruction. For an 8-point neighborhood system, the (i,j)th element of matrix C is given by

$$C_{i,j} = \begin{cases} 2(0.5\sqrt{2}+1)^{-1} & \text{if } \ d(i,j)=1 \\ 2(\sqrt{2}+1)^{-1} & \text{if } \ d(i,j)=\sqrt{2} \\ 0 & \text{otherwise} \end{cases},$$

where $d(i,j)$ is the Euclidean distance between pixels i and j, and $|\phi| < 1/8$. Note that $\sum_j C_{i,j} = 8$

If we assume a "toroidal edge correction", we now introduce the line process by rewriting (3) as

$$
\begin{aligned}
&-\log P(X,L) \propto \\
&\propto \frac{\alpha\phi}{2}\sum_i C_{i,i:1}(x_i - x_{i:1})^2(1-l_{[i,i:1]}) + \frac{\alpha\phi}{2}\sum_i C_{i,i:2}(x_i - x_{i:2})^2(1-l_{[i,i:2]}) \\
&+ \frac{\alpha\phi}{2}\sum_i C_{i,i:5}(x_i - x_{i:5})^2(1-l_{[i,i:5]}) + \frac{\alpha\phi}{2}\sum_i C_{i,i:6}(x_i - x_{i:6})^2(1-l_{[i,i:6]}) \\
&+ \frac{\alpha}{2}\sum_i \beta\left[l_{[i,i:1]} + l_{[i,i:2]} + l_{[i,i:5]} + l_{[i,i:6]}\right] + \frac{\alpha}{2}\sum_i (1-8\,\phi)x_i^2, \qquad (4)
\end{aligned}
$$

where $i{:}1,\ i{:}2, ...,\ i{:}8$ are the eight pixels around pixel i (see Fig. 1). The element $l([i,j])$ takes the value zero if pixels i and j are not separated by an active line and one otherwise. The parameter β is a scalar weight, which adjusts the introduction of active lines or edges in the image. For very large β the prior model becomes Gaussian. The process line acts as inhibitor or activator of the relation between two neighboring pixels depending on whether or not there exists an edge. We note that the CAR model is obtained when $l[i,j] = 0, \forall i,j$.

3 MAP Estimation

Let us now proceed to find $\hat{X}$, $\hat{L}$, the MAP estimates of X and L which are given by the following equation

$$\hat{X}, \hat{L} = \arg\max_{X,L} P(X,L|Y). \qquad (5)$$

The joint probability distribution $P(X,L|Y)$ is nonlinear, therefore it is difficult to find $\hat{X}$ and $\hat{L}$ by conventional methods since these procedures do not usually reach the global minimum of the energy function. Therefore stochastic algorithms such as simulated annealing have been proposed (see [6, 15]). In this work, the method we use for estimating the original image and the line process is stochastic for the line process and deterministic for the reconstruction.

In order to estimate the line process we simulate the corresponding conditional *a posteriori* density function. Let us denote by $P_T(l_{[i,j]}|L_{[i,j]}, X, Y)$ the conditional *a posteriori* density function for the line process $l_{[i,j]}$, given X, Y and the rest of L, $L_{[i,j]} = (l_{[s,t]} : \forall [s,t] \neq [i,j])$. To simulate this density function, we have the following equations

$$P_T(l_{[i,j]} = 0|L_{[i,j]}, X, Y) \propto \exp\left[-\frac{1}{T}\frac{\alpha\phi}{2}(x_i - x_j)^2\right] \qquad (6)$$

$$P_T(l_{[i,j]} = 1|L_{[i,j]}, X, Y) \propto \exp\left[-\frac{1}{T}\frac{\alpha\beta}{2}\right], \qquad (7)$$

where T is the temperature. Equation (6) shows the likelihood to obtain an active line element, whereas (7) just represents the opposite.

Given an estimate of the line process, L, and the observation, Y, we note that $P(X|L,Y)$ is convex and quadratic so that a deterministic method can be used

to estimate the image X. This method starts by differentiating the function $-\log P(X|L,Y)$ with respect to each pixel x_i, and so we have the following equation

$$
\begin{aligned}
-\frac{\partial}{\partial x_i}\log P(X|L,Y) &= \alpha(1-8\phi)x_i + \\
&+ \alpha\phi x_i \sum_{j\in\mathcal{N}_i} C_{i,j}(1-l_{[i,j]}) - \alpha\phi \sum_{j\in\mathcal{N}_i} C_{i,j}x_j(1-l_{[i,j]}) \\
&+ \sum_{s=1}^{M} y_s A_{s,i} - \sum_{s=1}^{M} b_s A_{s,i} e^{-\sum_{j=1}^{N} A_{s,j}x_j} = 0,
\end{aligned}
$$

where $j \in \mathcal{N}_i$ denotes the neighboring pixels of i

Taking into account that $\phi\sum_{j\in\mathcal{N}_i} C_{i,j} + (1-8\,\phi) = 1$ and noting that when $l_{[i,j]} = 1$, both $x_i(1-l_{[i,j]})$ and $x_j(1-l_{[i,j]})$ are zero, we have at the minimum of the function $-\log P(X|L,Y)$

$$
\begin{aligned}
\alpha x_i + \sum_{s=1}^{M} y_s A_{s,i} = \alpha\phi \sum_{j\in\overline{\mathcal{N}}_i} x_j C_{i,j} + \alpha\phi x_i \sum_{j\in\underline{\mathcal{N}}_i} C_{i,j} + \\
+ \sum_{s=1}^{M} b_s A_{s,i} e^{-\sum_{j=1}^{N} A_{s,j}x_j},
\end{aligned}
\tag{8}
$$

where $\overline{\mathcal{N}}_i$ and $\underline{\mathcal{N}}_i$ denote, respectively, the neighboring pixels of i without and with an active line between i and j. We have removed their dependency on the current line process estimate for simplicity.

Multiplying both sides of the Eq. (8) by x_i, we obtain

$$
x_i = x_i \frac{\alpha\mu_i(X) + \sum_{s=1}^{M} b_s A_{s,i} e^{-\sum_{j=1}^{N} A_{s,j}x_j}}{\alpha x_i + \sum_{s=1}^{M} y_s A_{s,i}},
\tag{9}
$$

with

$$
\mu_i(X) = \phi \sum_{j\in\overline{\mathcal{N}}_i} x_j C_{i,j} + \phi x_i \sum_{j\in\underline{\mathcal{N}}_i} C_{i,j}.
$$

Equation (9) is a characteristic function, hence it describes an iterative process for the image estimation. We note that the backprojections of the observations $\sum_{s=1}^{M} y_s A_{s,i}$ need only be determined once. We also note that when $\alpha = 0$ we obtain a maximum likelihood expectation maximization (ML-EM) algorithm.

Let us now consider the ordered subsets (OS) principle. The principle was introduced to reduce the reconstruction time of the classical ML-EM algorithm for emission tomography [9]. The OS technique can be applied to any algorithm that involves sums over sinogram indices by replacing them with sums over a subset

of projection data, consequently it is widely used to improve the convergence of iterative reconstruction methods [4, 8, 12].

Now, we use OS to speed up the iterative procedure in (9). We denote by U the number of subsets $V_1, ..., V_U$ chosen in the projection domain. We assume that the subsets cover the whole projection domain, they have the same size, and also that $V_a \bigcap V_b = \emptyset$ for $a \neq b$. We have

$$\sum_{s=1}^{M} b_s A_{s,i} e^{-\sum_{j=1}^{N} A_{s,j} x_j} = \sum_{u=1}^{U} \sum_{s \in V_u} b_s A_{s,i} e^{-\sum_{j=1}^{N} A_{s,j} x_j}, \quad \forall i \tag{10}$$

and

$$\sum_{s=1}^{M} y_s A_{s,i} = \sum_{u=1}^{U} \sum_{s \in V_u} y_s A_{s,i}, \quad \forall i. \tag{11}$$

We now use the following approximations

$$\sum_{s=1}^{M} b_s A_{s,i} e^{-\sum_{j=1}^{N} A_{s,j} x_j} \approx U \sum_{s \in V_u} b_s A_{s,i} e^{-\sum_{j=1}^{N} A_{s,j} x_j}, \quad \forall i \tag{12}$$

and

$$\sum_{s=1}^{M} y_s A_{s,i} \approx U \sum_{s \in V_u} y_s A_{s,i}, \quad \forall i. \tag{13}$$

The OS version of (9) then becomes

$$\begin{aligned} x_i &= x_i \frac{\alpha \mu_i(X) + U \sum_{s \in V_u} b_s A_{s,i} e^{-\sum_{j=1}^{N} A_{s,j} x_j}}{\alpha x_i + U \sum_{s \in V_u} y_s A_{s,i}} \\ &= x_i \frac{\frac{\alpha}{U} \mu_i(X) + \sum_{s \in V_u} b_s A_{s,i} e^{-\sum_{j=1}^{N} A_{s,j} x_j}}{\frac{\alpha}{U} x_i + \sum_{s \in V_u} y_s A_{s,i}}, . \end{aligned} \tag{14}$$

In this expression, U takes the role of a scale factor which ensures that the selection of the hyperparameter α for the reconstruction does not depend on the number of subsets.

We can use (6), (7) and (14) in the following algorithm to find the MAP estimate of L and X:

Let $k = 1, 2, ...,$ be the sequence of iterations in which the lines or pixels are visited for updating.

1. Set $k = 0$ and assign an initial configuration denoted as X_{-1}, L_{-1}, and an initial temperature $T = 1$.
2. The evolution $\hat{L}_{k-1} \rightarrow \hat{L}_k$ of the whole line process is simulated by the probability functions defined in (6) and (7).
3. The evolution $\hat{X}_{k-1} \rightarrow \hat{X}_k$ of the whole image is obtained as:

(a) Set $\hat{F}_0 = \hat{X}_{k-1}$.
(b) For each subset V_u (where $u = 1, ..., U$) the evolution $\hat{F}_{u-1} \rightarrow \hat{F}_u$ is calculated by using $\hat{F}_{u-1}$ in the right hand side of (14) to obtain $\hat{F}_u$ in the left hand side of the same equation.
(c) Update the image estimate as $\hat{X}_k = \hat{F}_U$.

4. Set $k = k+1$. Decrease the temperature T according to an annealing scheme [10]

$$T = \frac{0.6}{\log(1+k)},$$

and go to step 2 until a stopping criterion is met.

4 Experimental Results

The proposed reconstruction method was applied to real PET transmission data. These data are available in [5] and represent a PET scan of an anthropomorphic torso phantom (Data Spectrum Corporation) that includes 3 attenuation levels: lungs, bone, and soft tissue. The blank and transmission scan has 192 angles and 160 radial bins and the size of the reconstructed attenuation map is 128×128 pixels.

The method was implemented with 1, 2, 4, 8, 16, 32, and 64 non overlapping subsets and henceforth, we denote the proposed algorithm by CGMRF_OSu with u the number of subsets. In the experiments, we adopt a balanced order of the subsets [9] such that projection angles corresponding to two adjacent indices for subsets are separated by angles with maximum angular distance. Figures. 2(a), 2(c), 2(d) and 2(e) show respectively the CGMRF_OS1, CGMRF_OS8, CGMRF_OS32 and CGMRF_OS64 reconstructions of the transmission map. Figures 2(b) and 2(f) shows the corresponding line process for the CGMRF_OS1 and CGMRF_OS64 reconstructions. We note that the method locates all regions in the image and the general form of the objects is clearly distinguished.

For all CGMRF_OSu cases, the parameters were experimentally chosen to be equal to $\alpha = 600000$ and $\beta = 8 \times 10^{-6}$, which capture all edges present in the image.

Using as stopping criterion

$$||\hat{X}_k - \hat{X}_{k-1}||^2 / ||\hat{X}_k||^2 < 10^{-7}, \tag{15}$$

the number of iterations needed for each CGMRF_OS reconstruction are shown in table 1. We can see that the number of iterations decreases when the number of subsets increases.

To compare the convergence speed, we applied the OSEM algorithm derived from Eq. (14) when $\alpha = 0$. The number of iterations for each OSEM reconstruction is also shown in table 1. In our experiment, the OSEM algorithm with 32 and 64 subsets significantly magnifies the noise after only one iteration and

therefore these cases are not considered. For OSEM, the quality of the reconstructed images depends on the number of projections in each subset; if we use a large number of subsets the reconstructed images are very sensitive to noise [19, 20]). Regularization allows us to use more subset levels (32 and 64) and improves the convergence of CGMRF_OS1, CGMRF_OS2, CGMRF_OS4, and CGMRF_OS8 in comparison to their OSEM versions.

For visual comparison, since the original image is obviously not available, we also show the reconstructions obtained by filtered back-projection (FBP), maximum likelihood (ML) without post-filtering, and also when conditional autorregresive (CAR) and generalized Gauss Markov random fields (GGMRF) prior image models are used (see respectively Figs. 3(a), 3(b), 3(c) and 3(d)).

For the last two reconstructions, the scale parameters were set to $\alpha = 8500$ (CAR) and $\sigma^p = 0.0058$ for a shape parameter $p = 1.1$ (GGMRF) (we note that $\sigma^2 = 1/\alpha$ [2]). Scale parameters were obtained using the hyperparameter estimation process described in [14]. It can be observed that the use of a CAR prior penalizes excessively the edges (see Fig. 3(c)), while both the GGMRF and the proposed CGMRF_OS method better preserve them (see Figs. 2(a), 2(c), 2(d), 2(e) and 3(d)).

The CAR prior is a special case of both the GGMRF and CGMRF priors. The CAR prior corresponds to a GGMRF prior when the shape parameter is equal to 2 and, as noted previously, the CGMRF is equivalent to the CAR prior when β is very large. Note that, in the presence of edges, the variance of the prior distribution (the inverse of the parameter α), is greater for the CAR prior than for the CGMRF one. Since the CAR prior does not take into account the presence of edges, the variance of the model increases due to the difference between the pixel in both sides of an edge. However, the CGMRF prior takes into account that pixels across the edges are not related and, hence, the variance of the model decreases.

5 Conclusions

In this paper we have presented a new method for the reconstruction of transmission images. This method uses a compound Gauss Markov random field as prior model. This prior is particularly well adapted to the characteristics of these images. MAP estimation is performed by simulated annealing for the line process and a deterministic iterative scheme for the transmission image reconstruction, which utilizes ordered subsets for the image update. According to our experimental results, the proposed Bayesian method provides an acceptable acceleration and increases the quality of the reconstruction with respect to FBP, OSEM, CAR and GGMRF algorithms, since regions with differents values of attenuation can be better distinguished.

References

1. Bai, C., Kinahan, P.E., Brasse, D., Comtat, C., Townsend, D.W.: Post-injection Single Photon Transmission Tomography with Ordered-Subset Algorithms for Whole-

Table 1. Number of iterations

	OS1	OS2	OS4	OS8	OS16	OS32	OS64
CGMRF_OS	155	110	101	88	79	50	37
OS-EM	343	242	167	113	75	–	–

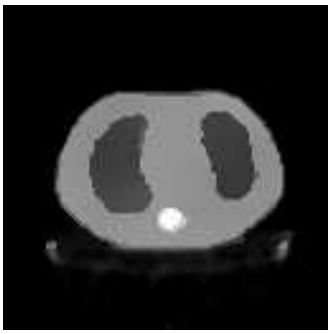

(a) CGMRF_OS1

(b) Line process OS1

(c) CGMRF_OS8

(d) CGMRF_OS32

(e) CGMRF_OS64

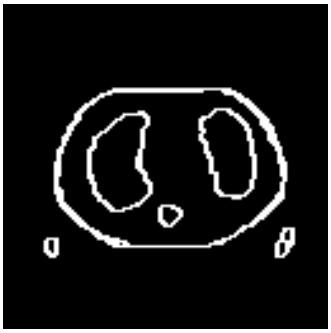

(f) Line process OS64

Fig. 2. Results with transmission real data

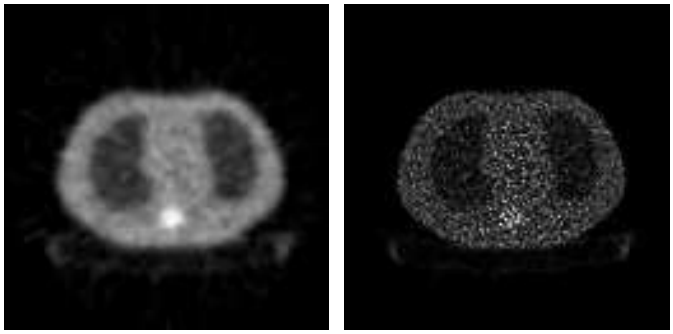

(a) FBP reconstruction (b) EM-ML reconstruction

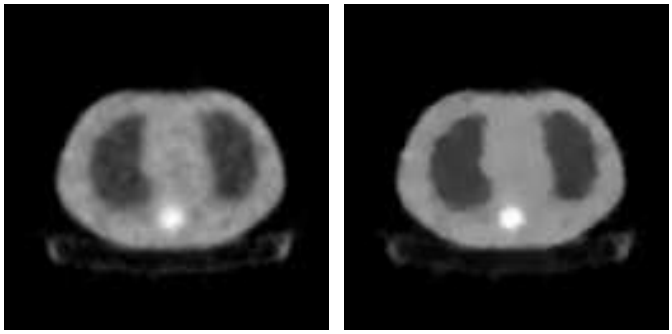

(c) CAR reconstruction (d) GGMRF reconstruction

Fig. 3. Results with transmission real data

Body PET Imaging. IEEE Tr. Nucl. Sci. **49** (2002) 74–81

2. Bouman, C.A., Sauer, K.: A Generalized Gaussian Image Model for Edge-Preserving Map Estimation. IEEE Tr. Im. Proc. **2** (1993) 296–310
3. Byrne, C.L.: Accelerating the EMML algorithm and related iterative algorithms by rescaled block-iterative methods. IEEE Tr. Im. Proc. **7** (1998) 100–109
4. Erdogan, H., Fessler, J.A.: Monotonic Algorithms for Transmission Tomography. IEEE Tr. Med. Im. **18** (1999) 801–14
5. J.A. Fessler, ASPIRE (A Sparse Precomputed Iterative Reconstruction Library), http://www.eecs.umich.edu/~fessler/aspire/index.html
6. Geman, S., Geman, G.: Stochastic Relaxation, Gibbs Distributions, and the Bayesian restoration of Images. IEEE Tr. Patt. Anal. Mach. Intell. **6** (1984) 721–741
7. R.E. Henk, Editor: The Scientific Basis of Nuclear Medicine. Second Edition. Mosby (1996).
8. Hsiao, I.-T., Rangarajan, A., Khurd, P., Gindi, G.: An Accelerated Convergent Ordered Subsets Algorithm for Emission Tomography. Phys. Med. Biol. **49** (2004) 2145–2156
9. Hudson, H.M., Larkin, R.S.: Accelerated Image Reconstruction Using Ordered Subsets of Projection Data. IEEE Tr. Med. Im. **4** (1994) 601–609
10. Jeng, F.C., Woods, J.W.: Simulated Annealing in Compound Gaussian Random Fields. IEEE Tr. Inform. Th. **36** (1988) 94–107

11. Kak, A.C., Slaney, M.: Principles of Computerized Tomographic Imaging. IEEE Press (1988)
12. Lee, S.-J.: Accelerated Deterministic Annealing Algorithms for Transmission CT Reconstruction Using Ordered Subsets. IEEE Tr. Nucl. Sci. **49** (2002) 2373–2380
13. López, A., Molina, R., Mateos, J., Katsaggelos, A.K.: SPECT Image Reconstruction Using Compound Prior Models. Int. J. Pattern Recognit. Artif. Intell. **16** (2002) 317–330
14. López, A., Molina, R., Katsaggelos, A.K.: Bayesian Reconstruction for Transmission Tomography with Scale Hyperparameter Estimation. Lecture Notes in Computer Science LNCS **3523** (2005) 455-462
15. Molina, R., Katsaggelos, A.K., Mateos, J., Hermoso, A., Segall, C.A.: Restoration of Severely Blurred High Range Images Using Stochastic and Deterministic Relaxation Algorithms in Compound Gauss-Markov Random Fields. Patt. Recogn. **33** (2000) 557–571
16. Molina, R., Mateos, J., Katsaggelos, A.K., Vega, M.: Bayesian Multichannel Image Restoration Using Compound Gauss-Markov Random Fields. IEEE Tr. Im. Proc. **12** (2003) 1642–1654
17. Oskoui-Fard, P., Stark, H.: Tomographic Image Reconstruction Using the Theory of Convex Projections. IEEE Tr. Med. Im. **7** (1988) 45–58.
18. Ripley, B.: Spatial Statistic. Wiley New York (1981)
19. Takahashi, M., Ogawa, K.: Selection of Projection Set and the Ordered of Calculation in Ordered Subsets Expectation Maximization Method. IEEE Nucl. Scie. Symp. and Med. Imag. Conf. Rec. **2** (1997) 1408–1412
20. Urabe, H., Ogawa, K.: Improvement of Reconstructed Images in Ordered Subsets Bayesian Reconstruction Method. IEEE Nucl. Scie. Symp. and Med. Imag. Conf. Rec. **2** (1998) 1342–1346
21. Yu, D.F., Fessler, J.A.: Edge-preserving Tomographic Reconstruction with Nonlocal Regularization. IEEE Tr. Med. Im. **21** (2002) 159–173